Signal strength regulates antigen-mediated T-cell deceleration by distinct mechanisms to promote local exploration or arrest

Hélène D. Moreau, Fabrice Lemaître, Kym R Garrod, Zacarias Garcia, Ana-Maria Lennon-Duménil, Philippe Bousso

HAL Id: pasteur-01238129
https://pasteur.hal.science/pasteur-01238129

Submitted on 4 Dec 2015

Signal strength regulates antigen-mediated T-cell deceleration by distinct mechanisms to promote local exploration or arrest

Hélène D. Moreau[a,b,c], Fabrice Lemaître[a,b], Kym R. Garrod[a,b], Zacarias Garcia[a,b], Ana-Maria Lennon-Duménil[d], and Philippe Bousso[a,b,1]

[a]Dynamics of Immune Responses Unit, Institut Pasteur, 75015 Paris, France; [b]INSERM U668, 75015 Paris, France; [c]Cellule Pasteur, Sorbonne Paris Cité, University Paris Diderot, 75015 Paris, France; and [d]INSERM U932, Institut Curie, 75005 Paris, France

T lymphocytes are highly motile cells that decelerate upon antigen recognition. These cells can either completely stop or maintain a low level of motility, forming contacts referred to as synapses or kinapses, respectively. Whether similar or distinct molecular mechanisms regulate T-cell deceleration during synapses or kinapses is unclear. Here, we used microfabricated channels and intravital imaging to observe and manipulate T-cell kinapses and synapses. We report that high-affinity antigen induced a pronounced deceleration selectively dependent on Ca^{2+} signals and actin-related protein 2/3 complex (Arp2/3) activity. In contrast, low-affinity antigens induced a switch of migration mode that promotes T-cell exploratory behavior, characterized by partial deceleration and frequent direction changes. This switch depended on T-cell receptor binding but was largely independent of downstream signaling. We propose that distinct mechanisms of T-cell deceleration can be triggered during antigenic recognition to favor local exploration and signal integration upon suboptimal stimulus and complete arrest on the best antigen-presenting cells.

T cell | kinapse | synapse | migration

Vigorous cellular motility is a critical property of T cells that constantly survey secondary lymphoid organs and peripheral tissues in search of cognate antigen. At steady state, T cells migrate in lymph nodes at 12–15 µm/min in a pattern best described as a "guided random walk," moving among the fibroblastic reticular cell (FRC) network in an apparent stochastic manner (1, 2). Upon encounter with an antigen-presenting cell (APC) harboring cognate antigen, T cells can adopt two types of behavior (3, 4). Under certain conditions, T-cell receptor (TCR) stimulation can lead to the complete arrest of T-cell migration and subsequent stable T cell–APC conjugation. This contact, also referred to as synapse, may last several hours and is promoted by high intracellular calcium signals (5, 6), although Ca^{2+} elevation may not always be required for T-cell arrest (7). Under other circumstances, T cells decelerate upon antigen encounter but do not completely stop migrating, only maintaining brief contact with the APC for a few minutes. Such transient and dynamic interactions have been termed kinapses (3). Kinapses can predominate in the early phases of T-cell activation (8–10) and are favored by TCR ligands of low potency or low affinity (6, 11). Kinapses can also be observed in the late phase of activation when T cells have been visualized swarming antigen-bearing APCs (1, 9) as well as during interactions between follicular helper T cells and germinal center B cells (12). At least in some instances, kinapses can result in measurable TCR signaling, as visualized by TCR internalization, Ca^{2+} elevation, and shedding of CD62L (11–14). Therefore, T cells can effectively couple motility and integration of activation signals. Although the formation of stable T cell–APC immunological synapses has been studied in detail, the molecular mechanisms driving kinapse behavior remain to be fully understood. In particular, it is not known whether T-cell deceleration during kinapses and synapses relies on the same molecular mechanisms. It is also unclear

whether kinapses simply reflect a slow version of T-cell steady-state migration or whether they are associated with a fundamentally different mode of motility.

To address these issues, we visualized and manipulated T-cell kinapses and synapses using two complementary approaches: (i) fabricated microchannels (15) to provide a 3D confined environment favoring T-cell motility in vitro (16) and (ii) intravital two-photon imaging of lymph nodes to study T cells in their native environment.

We found that high-affinity antigen triggered maximal T-cell deceleration that was selectively dependent on Ca^{2+} signals and actin-related protein 2/3 complex (Arp2/3) activity. By contrast, weak-affinity ligands promoted a switch of migration mode, characterized by partial deceleration and frequent direction changes that underlay the exploratory behavior of immunological kinapses. This switch required TCR binding to pMHC but was independent of intracellular TCR signals. Our results suggest that the action of distinct mechanisms tailors the level of T-cell deceleration to the antigenic stimulus to promote scanning of APCs with low stimulatory capacity and full arrest on highly stimulatory APCs.

Results

Low Velocity and Frequent Direction Changes During Kinapse Formation.
We have recently reported that TCR-pMHC affinity regulates T-cell dynamics in the spleen during antigen recognition, with low-affinity antigen favoring kinapses over synapses (11). To further characterize T-cell kinapses in vivo, we imaged OT-I CD8+ T cells in lymph nodes before and after injection with either the high-affinity antigenic peptide (N4) or the lower-affinity variant (Q4) (17). Consistent with our previous observations
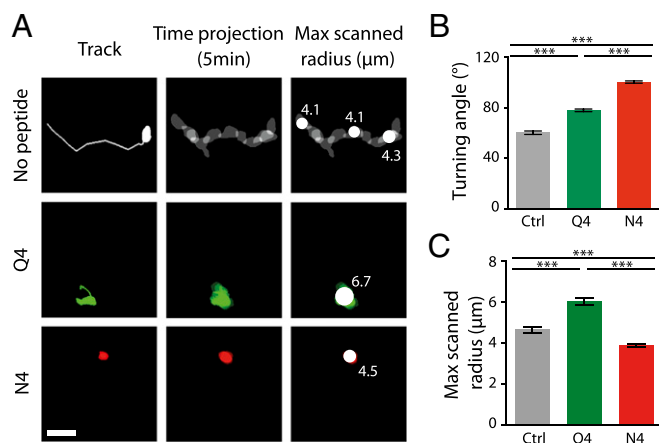
IMMUNOLOGY AND INFLAMMATION

Fig. 1. Frequent direction changes and increased exploration during kinapses in vivo. Mice were transferred with GFP$^+$ OT-I CD8$^+$ T cells, were injected with the high-affinity (N4) or the low-affinity (Q4) peptide, and were subjected to intravital imaging of the popliteal lymph node. (*A*) Recognition of low-affinity peptide is associated with efficient exploration of T cell's vicinity. T-cell images are projected over a 5-min trajectory. The maximal scanned radius was derived from the largest inscribed circle (white plain circle) in the projected track. (Scale bar: 20 μm.) (*B*) Turning angles measured in T-cell trajectories between two consecutive images (30 s apart). (*C*) Maximal scanned radius (μm) calculated for individual T cells. Data are representative of at least three independent experiments. ***$P < 0.001$.

in the spleen, N4 induced a complete (or near-complete) arrest of T-cell migration in lymph nodes. Q4 injection, however, resulted in only partial T-cell deceleration with maintenance of a motile behavior (Fig. S1 and Movie S1), reminiscent of kinapses. We further examined T-cell trajectories observed at steady state or during kinapses induced by the Q4 peptide. We found that upon recognition of this low-affinity ligand, T cells exhibited a more confined migration than that observed at steady state, characterized by more pronounced direction changes (Fig. S1 and Fig. 1 *A* and *B*). In fact, at steady state, individual T cells explored the lymph node over long distances but rarely scanned extensively a given neighborhood, leaving many areas unexplored. By contrast, the features of T-cell motility induced by recognition of the Q4 peptide suggested that kinapses are associated with the thorough exploration of the T cell's neighboring environment. This could represent an efficient strategy to scan the microenvironment in close vicinity of the initial antigen encounter. To test this idea, we considered that the largest circle inscribed in individual T-cell trajectories may represent the area fully scanned (in all directions) around the site of antigen recognition (Fig. 1*A*). We used the radius of this circle (maximal scanned radius) as an estimate of T cell thorough exploration. At steady state, T cells scanned small zones as they displayed relatively straight trajectories. The high-affinity N4 peptide promoted a very focused recognition within a confined area. Conversely, the low motility and direction changes observed with Q4 peptide resulted in the systemic exploration of larger contiguous areas (Fig. 1*C*).

This distinct pattern of migration during kinapses is likely imposed, in part, by the shape of the interacting APCs. In addition, it is also possible that ongoing stimulation by weak ligands intrinsically modifies the way T cells migrate and favors direction changes. To explore this possibility, we took advantage of microfabricated channels that provide a versatile approach to study T-cell antigen recognition in a confined environment (11, 15, 16). In particular, the microchannel assay offers the ability to analyze the effect of specific immobilized molecules (such as pMHC) on T-cell migration, to manipulate cell behavior through the addition of specific inhibitors, and to image T-cell dynamics at high resolution. We previously observed that OT-I T cells

migrating in microchannels coated with recombinant K^b-Q4 antigenic complexes partially reduced their velocity, whereas recognition of K^b-N4 antigenic complexes induced a near-complete T-cell arrest, results similar to our in vivo observations (11). To extend our findings, we imaged T cells with increased temporal resolution to closely examine their scanning behavior. As expected, antigen recognition in the channels induced T-cell deceleration and frequent direction changes that were most pronounced with the high-affinity peptide (Fig. 2*A*, Fig. S2, and Movie S2). To quantify the zone extensively scanned by individual T cells, we projected T-cell trajectories (over 30 min) and defined the maximal scanned length as the longest continuous segment for which each location is occupied for at least 2 min. Consistent with our in vivo observations, it was again the
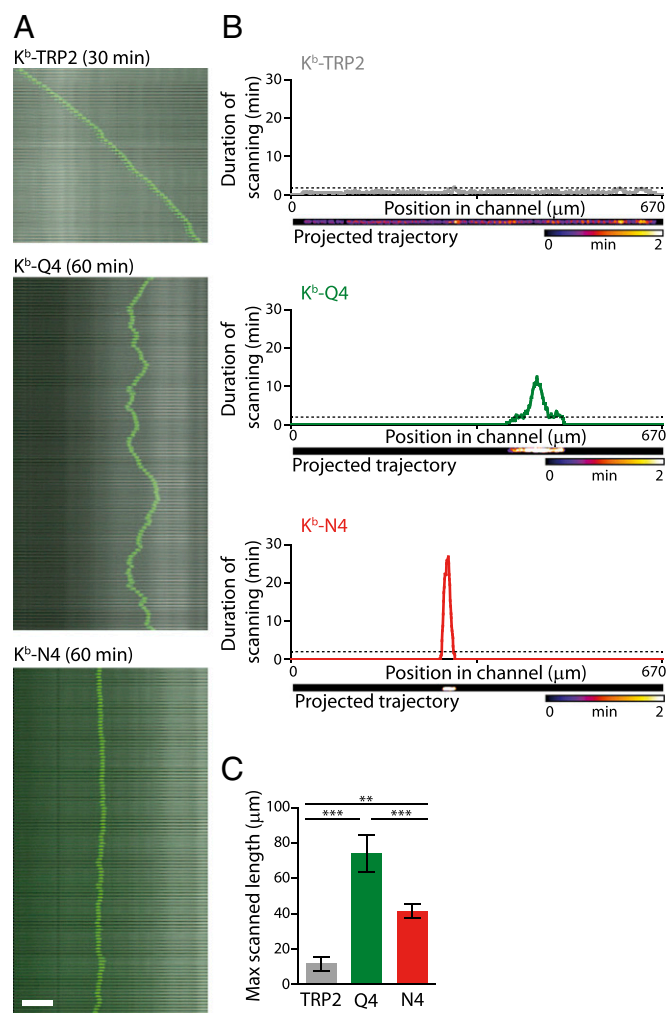
Fig. 2. Frequent direction changes and increased exploration during kinapses in microchannels. The migration of preactivated GFP$^+$ OT-I CD8$^+$ T cells was analyzed in 6-μm-wide microchannels coated with either K^b-TRP2 (control peptide), K^b-Q4, or K^b-N4 antigenic complexes. (*A*) Sequential images acquired every 35 s are shown for the indicated pMHC. (Scale bar: 100 μm.) (*B*) Examples of exploration in microchannels. T-cell images were subjected to thresholding and then projected over a 30-min trajectory. The duration of exploration is calculated at each pixel along the microchannel axis from the projected image. The maximal scanned length is defined as the longest continuous zone explored for more than 2 min (dotted line). (*C*) Average maximal scanned length calculated for T cells in each of the indicated conditions. Data are representative of five independent experiments. ***$P < 0.001$; **$P < 0.005$.

Fig. 3. Differential role of calcium influx during synapse versus kinapse formation. The migration of GFP^{+} OT-I CD8^{+} T cells was analyzed in pMHC-coated microchannels in the absence (−) or in the presence (+) of EGTA (extracellular Ca^{2+} chelator). (A) Sequential images acquired every 5 min are shown for the different conditions. (Scale 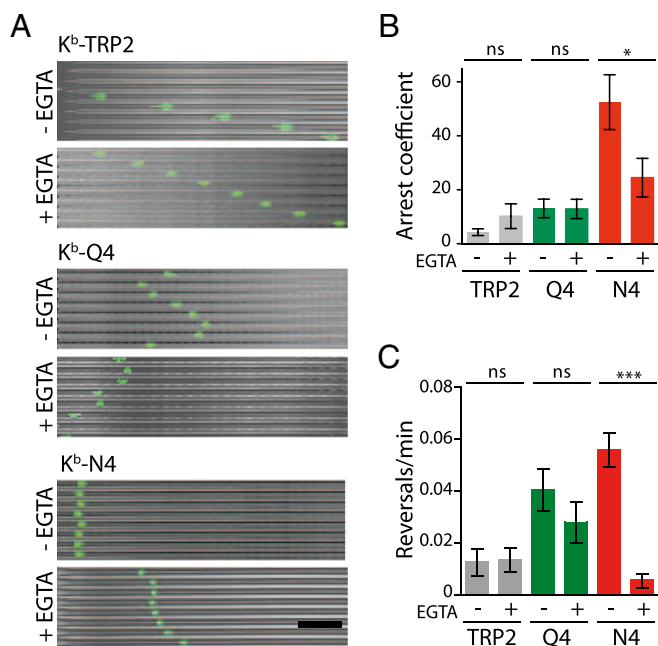bar: 50 μm.) (B and C) Arrest coefficients (B) and reversals per minute (C) are shown. Data are representative of five independent experiments. ***$P < 0.001$; *$P < 0.05$; ns, nonsignificant ($P > 0.05$).

lower-affinity peptide Q4 that promoted the thorough scanning of larger zones within the channels (Fig. 2 *B* and *C*). Altogether, these results support the premise that T cells adopt a scanning behavior upon recognition of low-affinity antigen, characterized by frequent direction changes and thorough exploration of their immediate environment.

Differential Role of Calcium Influx During Synapse Versus Kinapse Formation. We next examined whether similar or distinct mechanisms promoted T-cell deceleration induced by low- or high-affinity antigen. Extracellular calcium influx has been implicated in T-cell stop during antigen recognition (5, 6, 18). We therefore examined whether calcium signals are essential for T-cell behavior during kinapses. To this end, we imaged T-cell migration in microchannels coated with pMHC in the presence or absence of EGTA, an extracellular chelating agent (Fig. 3*A* and Movies S3–S5). We found that slow migration and frequent direction changes of T cells upon K^b-Q4 recognition was largely unaffected by the absence of extracellular calcium (Fig. 3 *B* and *C*). Similar results were obtained by chelating both extracellular and intracellular calcium with EGTA and BAPTA-AM, respectively (Fig. S3 *A* and *B*). These results suggest that calcium signals are not required for T-cell behavior during kinapses. In contrast, chelation of extracellular calcium limited the prominent T-cell deceleration observed with the high-affinity antigenic complex K^b-N4 (Fig. 3). Consistent with these observations, we observed robust calcium elevation in T cells stimulated with coated K^b-N4 complexes but little to no signals with K^b-Q4 (Fig. S3 *C* and *D*). In sum, we reveal a differential requirement for calcium signals during the formation of kinapses and synapses. Specifically, our results support the idea that low-affinity antigen induces a calcium-independent partial deceleration, whereas high-affinity antigen provides an additional calcium-dependent signal that facilitates T-cell arrest.

Distinct Requirements for Arp2/3 Activity During Synapse Versus Kinapse Formation. Actin remodeling is an important component of immunological synapse formation (19). Therefore, we assessed whether kinapse formation was equally dependent on actin dynamics. We analyzed T-cell migration in channels coated with K^b-TRP2, K^b-Q4, or K^b-N4 complexes in the presence of CK666, a known inhibitor of the Arp2/3 complex. Arp2/3 mediates the nucleation of branched actin. In the presence of the irrelevant K^b-TRP2 complex, T cells displayed fast and persistent migration that was only modestly altered by Arp2/3 inhibition (Fig. 4 and Movies S6–S8). Similarly, the partial T-cell deceleration observed in response to Q4 was largely unaffected by the inhibitor. However, the inhibitor reduced the robust T-cell deceleration induced by the high-affinity N4 antigen to a level comparable to that induced by the low-affinity antigen (Fig. 4 *B* and *C*). Altogether, these results further suggest the existence of distinct molecular mechanisms regulating T-cell deceleration during kinapses and synapses.

A Switch of Migration Mode During Kinapse Formation. The scanning behavior of T cells observed during kinapses suggested migration modalities distinct from steady state. To more completely investigate this possibility, we analyzed specific subcellular compartments of motile T cells in microchannels, namely the nucleus (labeled by Hoechst), the microtubule organizing center (MTOC) (labeled by expression of GFP-centrin), and the uropod. T cells placed in microchannels coated with an irrelevant antigenic complex (K^b-TRP2) harbored hallmarks of fast amoeboid migration, including the presence of a marked uropod (Fig. 5 *A* and *B*) and a MTOC localized at the trailing edge, along the central axis of the cell (Fig. 5 *C–E* and Movie S9). In sharp contrast, migrating T cells recognizing low-affinity antigenic complex lost their uropod and relocalized their MTOC close to the nucleus, toward the sides of the channel (Fig. 5 *A–E*
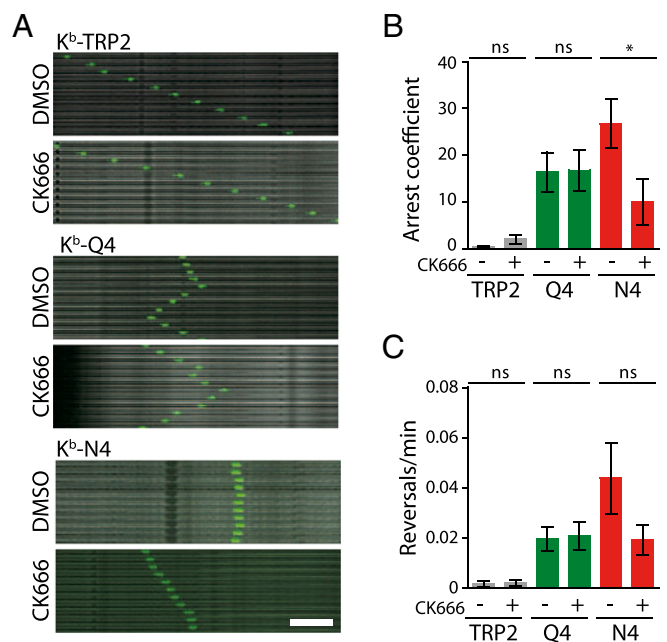
Fig. 4. Arp2/3 activity is required for T-cell arrest during synapses. The migration of GFP^{+} OT-I CD8^{+} T cells in pMHC-coated microchannels was analyzed in the presence of CK666 (inhibitor of Arp2/3) (+) or DMSO (−) as a control. (A) Sequential images acquired every 3 min are shown for the different conditions. (Scale bar: 50 μm.) (B and C) Arrest coefficients (B) and reversals per minute (C) are shown. Data are representative of five independent experiments. *$P < 0.05$; ns, nonsignificant ($P > 0.05$).
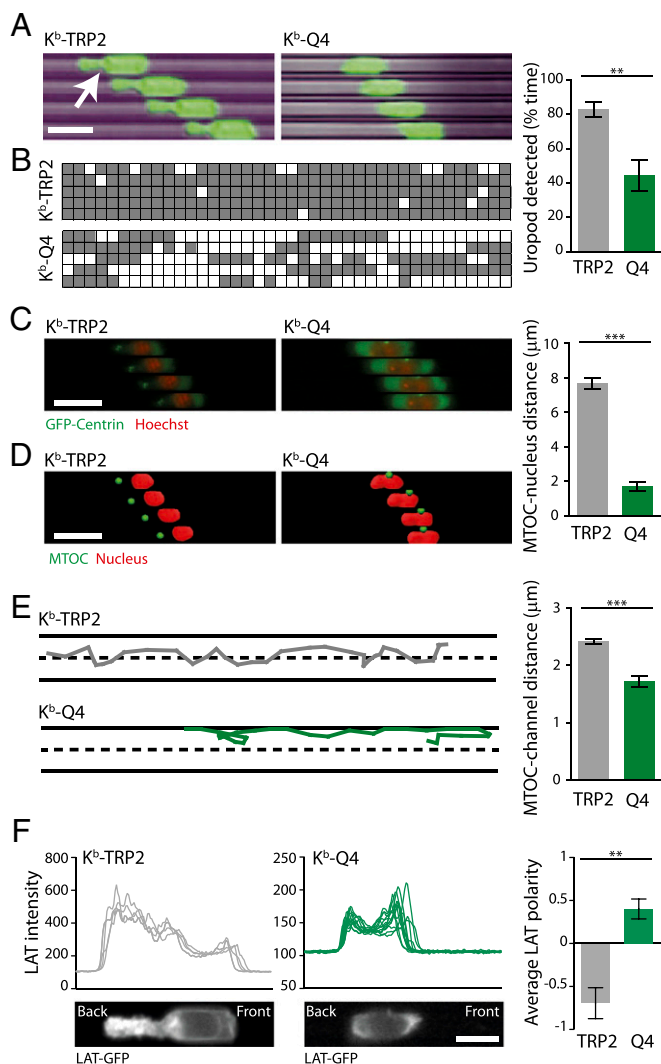
Fig. 5. Switch of migration mode during kinapse formation. (*A* and *B*) Recognition of low-affinity pMHC complexes results in T-cell migration in the absence of a marked uropod. The migration of preactivated GFP+ OT-I CD8+ T-cell was analyzed in pMHC-coated microchannels. (*A*) Sequential images acquired every 35 s are shown for the indicated pMHC. (Scale bar: 20 μm.) For each time point, cells were scored for the presence of a uropod (white arrow). (*B*) The presence of a uropod was analyzed for individual T cells. Each row represents one cell followed over time, and one square represents one time point. Filled squares correspond to time points in which a uropod was evident. The average percentage of time during which a uropod is detected is shown (*Right*). Data are representative of four independent experiments. (*C–E*) T-cell migration during recognition of low-affinity TCR ligands results in the relocation of the MTOC. OT-I CD8+ T cells were retrovirally transduced to express GFP-centrin and labeled with Hoechst. T-cell migration was analyzed in pMHC-coated microchannels. (*C*) Sequential images acquired every 35 s are shown for the indicated pMHC. Green indicates GFP-centrin; red indicates Hoechst. (Scale bar: 20 μm.) (*D*) Sequential images of MTOC and nucleus tracking. Green indicates MTOC; red indicates nucleus. (Scale bar: 20 μm.) The average distance between the MTOC and the nucleus is graphed (*Right*). (*E*) Representative trajectories of MTOC in a microchannel (gray and green lines). The black lines represent the microchannel sides, and the dotted line represents the microchannel axis. The average distance between the MTOC and the side of the microchannel is graphed (*Right*). Data are representative of four independent experiments. (*F*) T-cell migration during recognition of low-affinity TCR ligands results in the repolarization of LAT toward the front of the cell. (*Left*) Representative images of LAT-GFP–expressing OT-I T cells migrating in Kb-TRP2– or Kb-Q4–coated microchannels. (Scale bar: 10 μm.) Line scans of GFP intensity along the central axis of the microchannels are shown for different time points. (*Right*) Graph shows the average LAT polarity (−1: LAT at the rear of the cell; +1: LAT at

and Movie S10). We asked whether this mode of migration was also associated with the subcellular reorganization of TCR-associated molecules. We focused on a linker of activated T cells (LAT) protein that has been shown to be enriched in the uropod of migrating T cells. In T cells expressing a LAT-GFP fusion protein and migrating in control microchannels, fluorescence was largely restricted to the uropod region. However, a majority of LAT-GFP fluorescence was found at the front of T cells forming kinapses in Kb-Q4–coated microchannels (Fig. 5F and Movies S11 and S12). Altogether, these experiments establish the existence of distinct cellular organization patterns that differ in the presence of low-affinity peptide compared with steady-state conditions, strongly suggesting that a switch in the mode of migration underlies kinapse formation.

Partial T-Cell Deceleration During Kinapse Formation Requires TCR Binding to pMHC but Is Largely Independent of Downstream Signaling. The loss of uropod and reorientation of the MTOC toward the surface of the microchannel during kinapses were reminiscent of mesenchymal-like migration. In contrast, steady-state migration displayed the typical hallmarks of amoeboid motility. Because adhesion has been shown to favor mesenchymal over amoeboid behavior, we asked whether TCR binding to low-affinity antigenic complexes could be sufficient to slow down T cells and induce kinapses independently of intracellular TCR signaling. We therefore first evaluated the level of TCR signaling perceived by kinapse-forming T cells. We noted that T cells recovered from Kb-Q4–coated microchannel entrance had up-regulated CD69 and CD25 and down-regulated CD62L (Fig. S4). We also observed in microchannels that T cells expressing LAT-GFP showed punctuated LAT accumulations when recognizing cognate pMHC, with a tendency for less frequent and less persistent accumulations with the low-affinity pMHC complexes (Fig. S5 and Movies S12 and S13). These observations suggested that kinapses triggered by Kb-Q4 were inducing weak but productive signaling. To test whether these low levels of TCR signals were responsible for the partial T-cell deceleration seen with Kb-Q4, we analyzed T-cell migration in the presence of PP2, a well-characterized inhibitor of Src-family kinases. Although the presence of PP2 completely abrogated the activation of T cells by Kb-Q4 (Fig. S4), it did not prevent partial T-cell deceleration triggered by this antigenic complex (Fig. 6 and Movies S14–S16), nor the other hallmarks of kinapse motility (reversals and uropod loss; Fig. S6). Of note, PP2 inhibited the complete arrest mediated by high-affinity complexes (Fig. 6). Overall, our results suggest that TCR engagement acts by two mechanisms to promote T-cell deceleration: binding to pMHC may promote adhesion and switch of migration mode, whereas strong intracellular TCR signals are required for full arrest.

Discussion

Here, we have used two complementary assays to compare T-cell motility at steady state and during recognition of low-affinity antigen. To extend intravital imaging observations, we used microfabricated channels, a reductionist approach that reproduces in vivo confinement and allowed us to specifically visualize and interfere with T-cell recognition of pMHC complexes. Of note, this setting is versatile enough to include additional guidance cues or molecules present on the surface of dendritic cells or FRCs that also contribute to the regulation of T-cell dynamics in vivo.

At steady state, T cells harbor an amoeboid migration, characterized by high velocity and relatively persistent trajectories. This mode of migration allows individual T cells, in search of

the front of the cell). Data are representative of three independent experiments. ***P < 0.001; **P < 0.005.

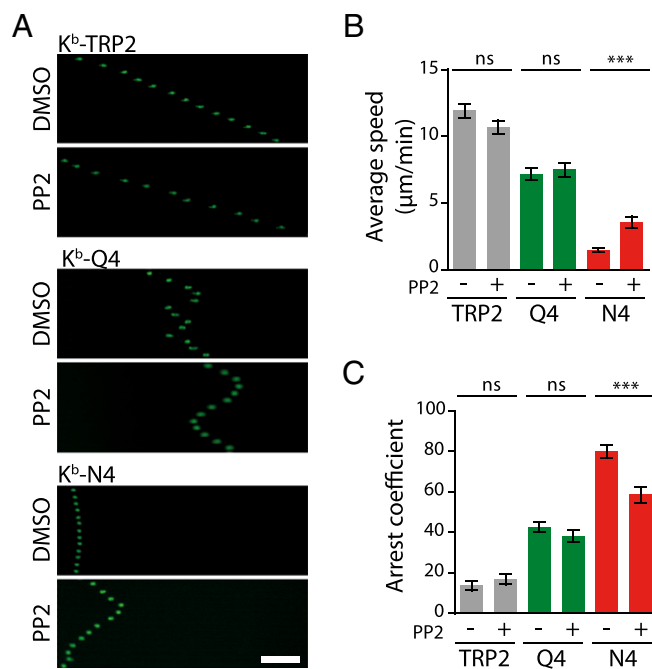**Fig. 6.** Kinapse formation requires TCR binding to cognate pMHC but appears largely independent of downstream signaling. The migration of GFP+ OT-I CD8+ T cells in pMHC-coated microchannels was analyzed in the presence of PP2 (Src-family kinases inhibitor) (+) or DMSO (−) as a control. (A) Sequential images acquired every 3 min are shown for the different conditions. (Scale bar: 40 μm.) (B and C) Average speed (B) and arrest coefficients (C) are shown. Data are representative of three independent experiments. ***$P < 0.001$; ns, nonsignificant ($P > 0.05$).

cognate antigen, to survey large territories of the lymph node. Suboptimal TCR stimulation induces kinapse formation, reflected by a switch of migration mode: T cells relocated their MTOC, lost their uropod, decreased their velocity, and changed direction more frequently. We would like to propose that this scanning behavior favors the integration of activation signals on the same APC or on APCs located in close proximity. Additionally, if TCR stimulation reaches a certain threshold, T cells fully stop and establish synapses by a mechanism dependent on Ca^{2+} and Arp2/3. Interestingly, the preferential requirement for Arp2/3 activity during synapse formation is consistent with the role of WASp in maintaining synapse stability (20). Such contribution of Arp2/3 could reflect the direct involvement of the actin-network or its recently described role in regulating PLC-γ1 and subsequent calcium signaling (21).

By dissecting T-cell migration in vitro on chamber slides coated with different substrates (but in the absence of cognate antigen), Krummel and colleagues have identified distinct crawling modes: amoeboid walking on casein-coated surface and haptokinetic sliding on ICAM-1–coated surface (22). Interestingly, the sliding mode was shown to be associated with increased adhesion. More recently, amoeboid to mesenchymal transition has been shown to be promoted by increased adhesion in a wide variety of cell types (23). Our results suggest that suboptimal TCR stimulation may be a physiological trigger for switching migration modes. In fact, the deceleration induced by low-affinity antigenic complexes was dependent on TCR engagement but appeared largely independent of downstream TCR signals. Recognition of low-affinity antigen may therefore result in an increased adhesion to the APC that would trigger a sliding/scanning type of migration and favor T-cell scanning of dendritic cells over FRCs. It remains possible that TCR signaling additionally interferes with molecular motors that are known to profoundly impact T-cell motility. During steady-state

migration, decreased myosin-IIA activity has been reported to promote an adhesive mode of crawling (16), whereas increased myosin-IG activity has been shown to favor direction changes (24).

Our results, together with previous studies, highlight the existence of diverse modes of migration for T cells in vivo (Fig. S7). We would like to propose that modulations in migratory behavior and calcium elevation induced by differential TCR stimulation potency represent an optimal strategy for T cells to increase signal integration and bind to the best APCs.

Materials and Methods

Mice. C57BL/6 mice were purchased from Charles River Laboratories. Rag1−/− OT-I TCR and *UBC*-GFP Rag1−/− OT-I TCR transgenic mice were bred in our animal facility. All mice were housed in our animal facility under specific pathogen-free conditions. Animal experiments were performed in accordance to institutional guidelines for animal care and use and approved by the Comité d'Ethique en Expérimentation Animale (CETEA) committee.

Peptides. The OVA$_{257–264}$ (N4) peptide (SIINFEKL), the Q4 variant peptide (SIIQFEKL), and the control peptide murine TRP2$_{180–188}$ (SVYEFFVWL) were purchased from Polypeptide Group.

T-Cell Migration Assay in Vivo. OT-I CD8+ T cells were isolated from the lymph nodes of *UBC*-GFP Rag1−/− OT-I mice and adoptively transferred into recipient C57BL/6 mice by i.v. injection. Two to 4 h after T-cell adoptive transfer, recipient mice were anesthetized and prepared for lymph node intravital imaging (25). Two-photon imaging was performed using a DM 6000B upright microscope equipped with a SP5 confocal head (Leica). Excitation was provided by a Chameleon Ultra Ti:Sapphire laser (Coherent) tuned at 950 nm. Emitted fluorescence was split using 562- and 495-nm dichroic mirrors and passed through 513/17 bandpass filter (Semrock) to a nondescanned detector (Leica). Typically, images from 8 to 12 z planes spaced 4 μm apart were collected every 30 s for up to 2 h. When indicated, recipient mice were injected i.v. with 50 μg of N4 or Q4 peptide 30–60 min after the beginning of image acquisition. Cell tracking was performed using the Imaris software (Bitplane). Straightness was calculated as the ratio of the distance from origin to the total distance traveled. The arrest coefficient was defined as the percentage of time the cell's instantaneous velocity was below 2 μm/min. The turning angle between two successive frames was calculated from the cell coordinates. The maximal scanned radius (normalized per time unit) was derived from the biggest inscribed circle in the maximum projection of 5-min-long cell tracks and measured using ImageJ.

T-Cell Migration Assay in pMHC-Coated Microchannels. GFP+ OT-I CD8+ T cells were preactivated in vitro for 72 h using anti-CD3/CD28 beads (Dynal) in the presence of 25 U/mL recombinant IL-2 (Roche) and allowed to migrate in 6-μm-wide microchannels coated with pMHC (11). In some experiments, T cells were retrovirally transduced to express GFP-centrin or LAT-GFP (26, 27) and stained with 1 μg/mL Hoechst 33342 (Life Technologies). In brief, OT-I T cells were activated for 2 d with anti-CD3/CD28 beads (Dynal) in the presence of 25 U/mL recombinant IL-2 (Roche) and spin-transduced at day 2 and day 3 after activation as previously described (27). When indicated, EGTA (2.5 mM; Sigma), CK666 (25 μM; Tocris), or PP2 (20 μM; Calbiochem) was added to the culture medium during the migration assay. For experiments with BAPTA-AM and PP2, cells were preloaded with BAPTA-AM (5 μM; Tocris) or PP2 (25 μM) for 30 min at 37 °C. In all experiments, solutions containing the indicated inhibitor were completely exchanged. Phase-contrast and fluorescence images were recorded every 30 s to 5 min for 10–12 h, using an DMI-6000B automated microscope (Leica) with a motorized stage (Pecon), an HQ2 Roper camera, and 10×/0.45 NA dry objective (Nikon) or 20×/0.75 NA dry objective (Olympus). The microscope was equipped with an environmental chamber for controlled temperature, humidity, and CO₂ (Pecon). Cell tracking was performed using the Imaris software (Bitplane). Movies were processed using ImageJ and Imaris. No obvious differences could be observed between the beginning and the end of the 12-h-long movies. Arrest coefficient was calculated as the percentage of time individual cells exhibited a velocity <2 μm/min. The maximal scanned length (normalized by time unit) in this assay was defined by projecting the cell images over a 30-min-long track and measuring the longest segment of microchannel on which the cell was projected for at least 2 min. Although the average values for motility parameters varied slightly in different experiments, the differences reported between the different peptides and

IMMUNOLOGY AND INFLAMMATION

conditions were always reproduced in several experiments. The presence of the uropod was scored based on the detection of an elongated structure at the rear of the cell, behind a marked constriction of the cytoplasm. The percentage of time during which individual cells exhibited a uropod was calculated on at least 10 consecutive time frames. The MTOC and nucleus were automatically tracked using Imaris. Distances between the MTOC and the nucleus or between the MTOC and the lateral borders of the microchannel were averaged for each cell using at least 10 consecutive time frames. LAT polarity was determined with a line scan (ImageJ plot profile) of the central axis of the microchannel. A value of −1 or +1 was attributed to the cell when LAT-associated fluorescence was maximal at the rear or at the front of the cell, respectively. The average LAT polarity for a given cell was calculated as the mean polarity over at least five time frames. The presence and persistence of LAT spots were quantified using ImageJ.

Flow Cytometry. T cells recovered from the entry port of the microchannels at the end of the experiment (12–16 h) were stained using APC-conjugated anti-CD69, BV421-conjugated anti-CD62L, and PE-Cy7–conjugated anti-CD25 mAb (BioLegend) and analyzed using a FACS Canto II and FlowJo (Tree Star).

Calcium Measurements in OT-I T Cells on pMHC-Coated Two-Dimensional Surfaces. Preactivated OT-I CD8^{+} T cells were stained with Fluo-3, AM (2.5 μM; Invitrogen) for 30 min at 37 °C and put in contact with surfaces coated with K^b-TRP2, K^b-Q4, or K^b-N4. As a positive control for Fluo-3 staining, ionomycin (500 ng/mL) was added to a noncoated well. Average Fluo-3 fluorescence was quantified for over 150 cells in each condition using ImageJ.

Statistical Analyses. Data are shown as means ± SEM. Statistical analyses were performed using a Mann–Whitney test or ANOVA, followed by a Tukey posttest (Prism version 5.0; GraphPad Software). Statistical significance is indicated as follows in the figures: ***$P < 0.001$; **$P < 0.005$; *$P < 0.05$; and ns, nonsignificant ($P > 0.05$).

1. Miller MJ, Wei SH, Parker I, Cahalan MD (2002) Two-photon imaging of lymphocyte motility and antigen response in intact lymph node. *Science* 296(5574):1869–1873.
2. Bajénoff M, et al. (2006) Stromal cell networks regulate lymphocyte entry, migration, and territoriality in lymph nodes. *Immunity* 25(6):989–1001.
3. Dustin ML (2008) T-cell activation through immunological synapses and kinapses. *Immunol Rev* 221:77–89.
4. Moreau HD, Bousso P (2014) Visualizing how T cells collect activation signals in vivo. *Curr Opin Immunol* 26:56–62.
5. Bhakta NR, Oh DY, Lewis RS (2005) Calcium oscillations regulate thymocyte motility during positive selection in the three-dimensional thymic environment. *Nat Immunol* 6(2):143–151.
6. Skokos D, et al. (2007) Peptide-MHC potency governs dynamic interactions between T cells and dendritic cells in lymph nodes. *Nat Immunol* 8(8):835–844.
7. Waite JC, et al. (2013) Interference with Ca(2+) release activated Ca(2+) (CRAC) channel function delays T-cell arrest in vivo. *Eur J Immunol* 43(12):3343–3354.
8. Mempel TR, Henrickson SE, Von Andrian UH (2004) T-cell priming by dendritic cells in lymph nodes occurs in three distinct phases. *Nature* 427(6970):154–159.
9. Miller MJ, Safrina O, Parker I, Cahalan MD (2004) Imaging the single cell dynamics of CD4+ T cell activation by dendritic cells in lymph nodes. *J Exp Med* 200(7):847–856.
10. Hugues S, et al. (2004) Distinct T cell dynamics in lymph nodes during the induction of tolerance and immunity. *Nat Immunol* 5(12):1235–1242.
11. Moreau HD, et al. (2012) Dynamic in situ cytometry uncovers T cell receptor signaling during immunological synapses and kinapses in vivo. *Immunity* 37(2):351–363.
12. Shulman Z, et al. (2014) Dynamic signaling by T follicular helper cells during germinal center B cell selection. *Science* 345(6200):1058–1062.
13. Gunzer M, et al. (2000) Antigen presentation in extracellular matrix: Interactions of T cells with dendritic cells are dynamic, short lived, and sequential. *Immunity* 13(3): 323–332.
14. Friedman RS, Beemiller P, Sorensen CM, Jacobelli J, Krummel MF (2010) Real-time analysis of T cell receptors in naive cells in vitro and in vivo reveals flexibility in synapse and signaling dynamics. *J Exp Med* 207(12):2733–2749.
15. Faure-André G, et al. (2008) Regulation of dendritic cell migration by CD74, the MHC class II-associated invariant chain. *Science* 322(5908):1705–1710.
16. Jacobelli J, et al. (2010) Confinement-optimized three-dimensional T cell amoeboid motility is modulated via myosin IIA-regulated adhesions. *Nat Immunol* 11(10): 953–961.
17. Zehn D, Lee SY, Bevan MJ (2009) Complete but curtailed T-cell response to very low-affinity antigen. *Nature* 458(7235):211–214.
18. Negulescu PA, Krasieva TB, Khan A, Kerschbaum HH, Cahalan MD (1996) Polarity of T cell shape, motility, and sensitivity to antigen. *Immunity* 4(5):421–430.
19. Ritter AT, Angus KL, Griffiths GM (2013) The role of the cytoskeleton at the immunological synapse. *Immunol Rev* 256(1):107–117.
20. Sims TN, et al. (2007) Opposing effects of PKCtheta and WASp on symmetry breaking and relocation of the immunological synapse. *Cell* 129(4):773–785.
21. Kumari S, et al. (2015) Actin foci facilitate activation of the phospholipase C-γ in primary T lymphocytes via the WASP pathway. *Elife* 4:e04953.
22. Jacobelli J, Bennett FC, Pandurangi P, Tooley AJ, Krummel MF (2009) Myosin-IIA and ICAM-1 regulate the interchange between two distinct modes of T cell migration. *J Immunol* 182(4):2041–2050.
23. Liu YJ, et al. (2015) Confinement and low adhesion induce fast amoeboid migration of slow mesenchymal cells. *Cell* 160(4):659–672.
24. Gérard A, et al. (2014) Detection of rare antigen-presenting cells through T cell-intrinsic meandering motility, mediated by Myo1g. *Cell* 158(3):492–505.
25. Celli S, Lemaître F, Bousso P (2007) Real-time manipulation of T cell-dendritic cell interactions in vivo reveals the importance of prolonged contacts for CD4+ T cell activation. *Immunity* 27(4):625–634.
26. Piel M, Meyer P, Khodjakov A, Rieder CL, Bornens M (2000) The respective contributions of the mother and daughter centrioles to centrosome activity and behavior in vertebrate cells. *J Cell Biol* 149(2):317–330.
27. Azar GA, Lemaître F, Robey EA, Bousso P (2010) Subcellular dynamics of T cell immunological synapses and kinapses in lymph nodes. *Proc Natl Acad Sci USA* 107(8): 3675–3680.

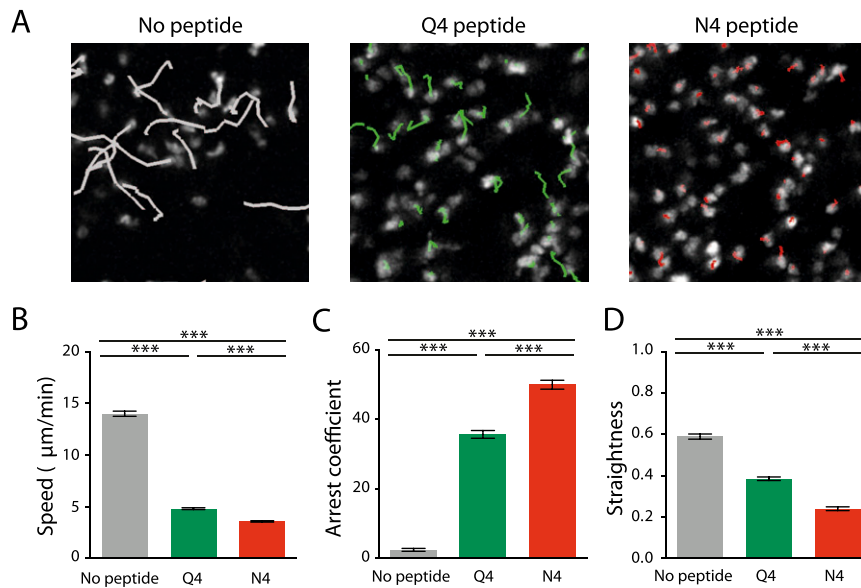# Supporting Information

Moreau et al. 10.1073/pnas.1506654112

Fig. S1. T-cell dynamics in the lymph node are regulated by TCR ligand affinity. Mice were transferred with GFP^{+} OT-I CD8^{+} T cells, were injected with the high-affinity (N4) or the low-affinity (Q4) peptide, and were subjected to intravital imaging of the popliteal lymph node. (*A*) Representative two-photon images and overlaid T-cell trajectories (corresponding to 5 min of imaging) in uninjected mice or mice receiving the Q4 or N4 peptide. (*B–D*) Average cell speed (μm/min) (*B*), arrest coefficient (percentage of time during which a cell exhibited an instantaneous speed <2 μm/min) (*C*), and straightness (*D*) are graphed. Data are representative of at least three independent experiments. ***$P < 0.001$.
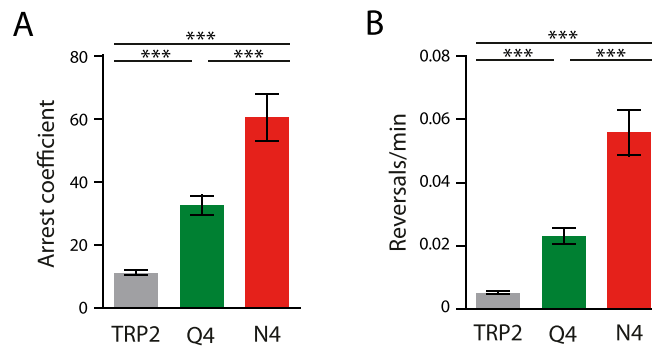

Fig. S2. Frequent direction changes and increased exploration during kinapses in microchannels. The migration of preactivated GFP^{+} OT-I CD8^{+} T cells was analyzed in 6-μm-wide microchannels coated with either K[b]-TRP2 (control peptide), K[b]-Q4, or K[b]-N4 antigenic complexes. (*A* and *B*) The average arrest coefficient (*A*) and number of reversals per minute (*B*) are shown for the indicated conditions. Data are representative of five independent experiments. ***$P < 0.001$.
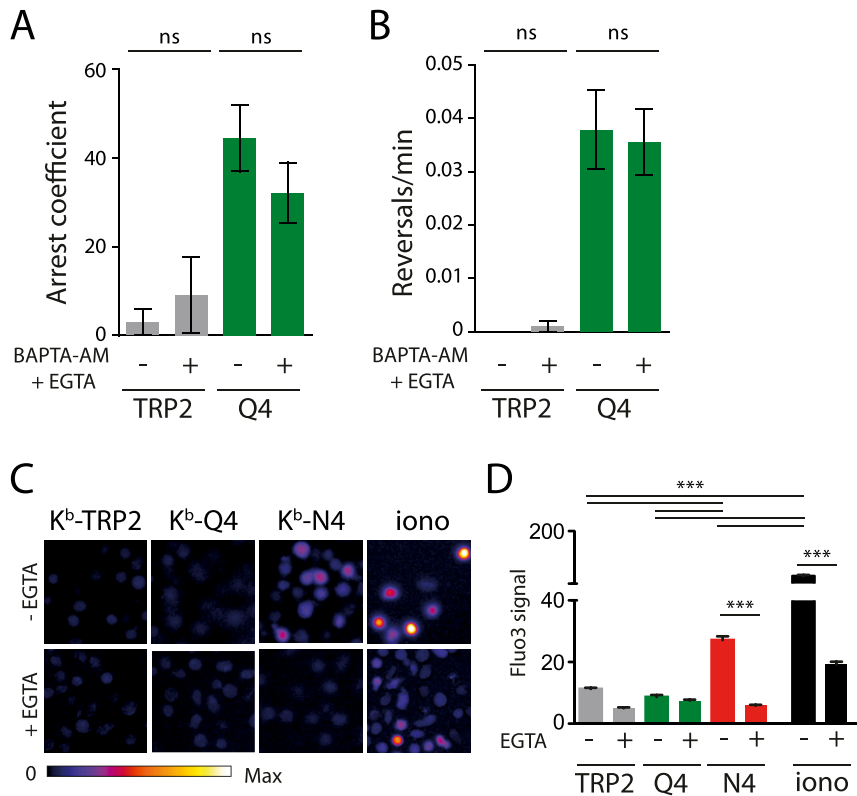
Fig. S3. T-cell deceleration does not require calcium signaling. Migration of GFP^{+} OT-I CD8^{+} T cells in pMHC-coated microchannels in the presence of BAPTA-AM (intracellular Ca^{2+} chelator) and EGTA (extracellular Ca^{2+} chelator) (+) or DMSO (−) as a control. (*A* and *B*) Arrest coefficients (*A*) and reversals per minute (*B*) are shown. Data are representative of three independent experiments. ns, nonsignificant ($P > 0.05$). (*C* and *D*) Only high-affinity pMHC induces a strong calcium influx, which is abolished in the presence of EGTA. OT-I CD8^{+} T cells were stained with a calcium indicator (Fluo-3) and stimulated with the indicated coated pMHC, in the absence or in the presence of EGTA to chelate extracellular calcium. (*C*) Representative images. (*D*) Average Fluo-3 signal detected in OT-I T cells in the different conditions of stimulation. Maximal response was estimated by stimulating the T cells with ionomycin. Only significant differences are noted. ***$P < 0.001$; ns, nonsignificant ($P > 0.05$).
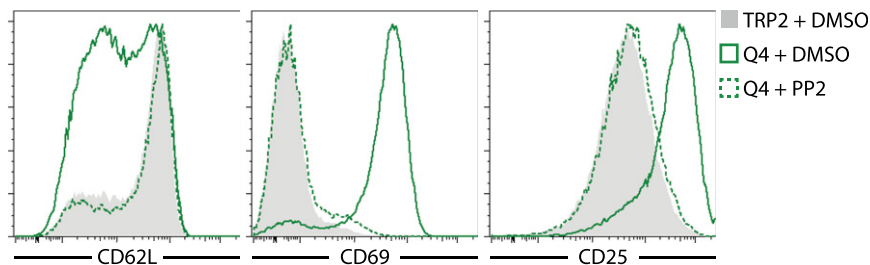

Fig. S4. PP2 effectively inhibits T-cell activation induced by K[b]-Q4 complexes. OT-I T cells recovered from the K[b]-Q4–coated microchannel entrance shows down-regulation of CD62L and up-regulation of CD69 and CD25 compared with the K[b]-TRP2 control. This activation signature was abolished by the addition of PP2.
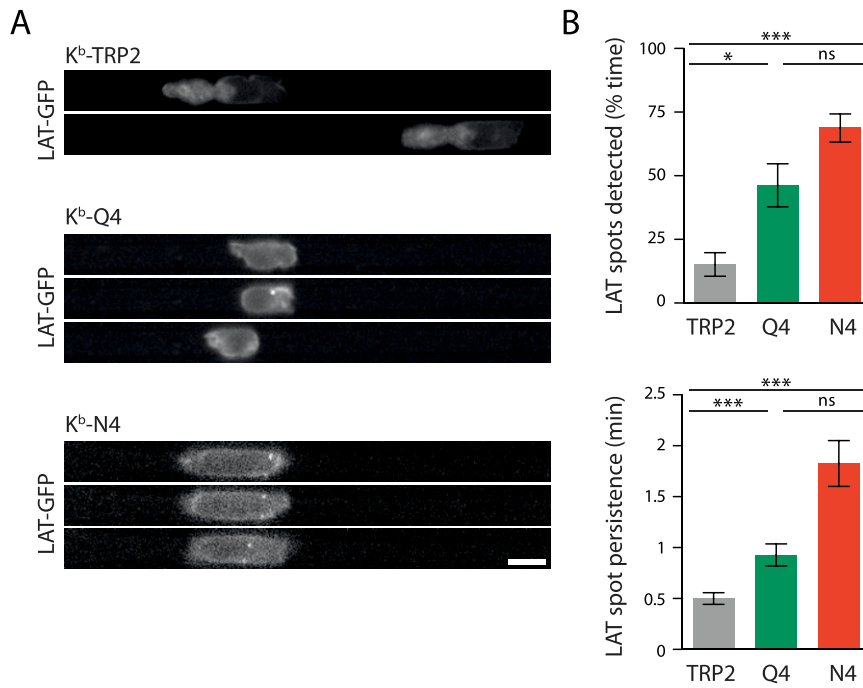
Fig. S5. Recognition of low- and high-affinity TCR ligands trigger LAT accumulations. (*A*) Representative images of LAT-GFP–expressing OT-I T cells migrating in K^b-TRP2–, K^b-Q4–, or K^b-N4–coated microchannels. LAT spots (bright punctuated GFP accumulations) can be observed on K^b-Q4 and K^b-N4 images. (Scale bar: 10 μm.) (*B*) Graphs show the average percentage of time during which LAT-punctuated accumulations were detected and the average persistence of the spots. Data are representative of three independent experiments. ***$P < 0.001$; *$P < 0.05$; ns, nonsignificant.
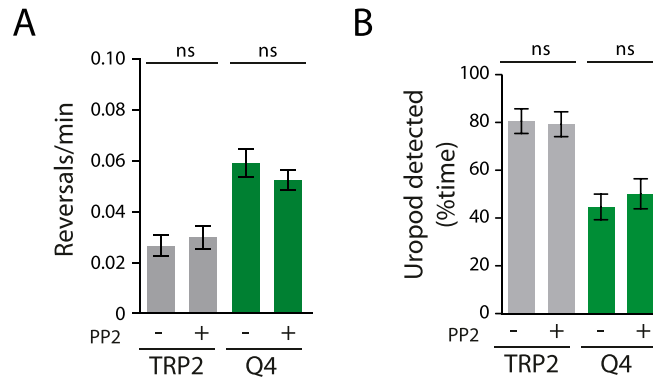

Fig. S6. The hallmarks of kinapse motility require TCR binding to pMHC but are largely independent of downstream TCR signaling. The migration of GFP⁺ OT-I CD8⁺ T cells in pMHC-coated microchannels was analyzed in the presence of PP2 (Src-family kinases inhibitor) (+) or DMSO (−) as a control. (*A* and *B*) The frequency of reversals (*A*) and the average percentage of time during which a uropod is detected (*B*) are shown. Data are representative of three independent experiments. ns, nonsignificant ($P > 0.05$).
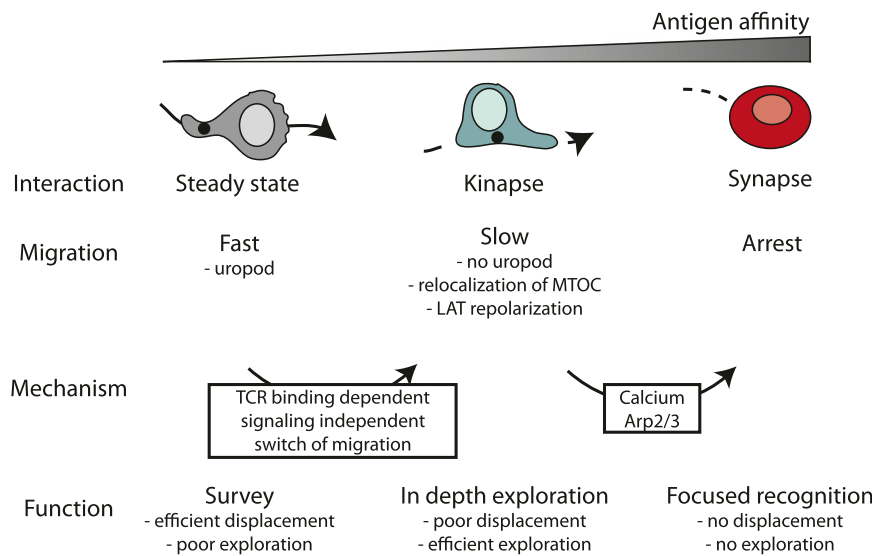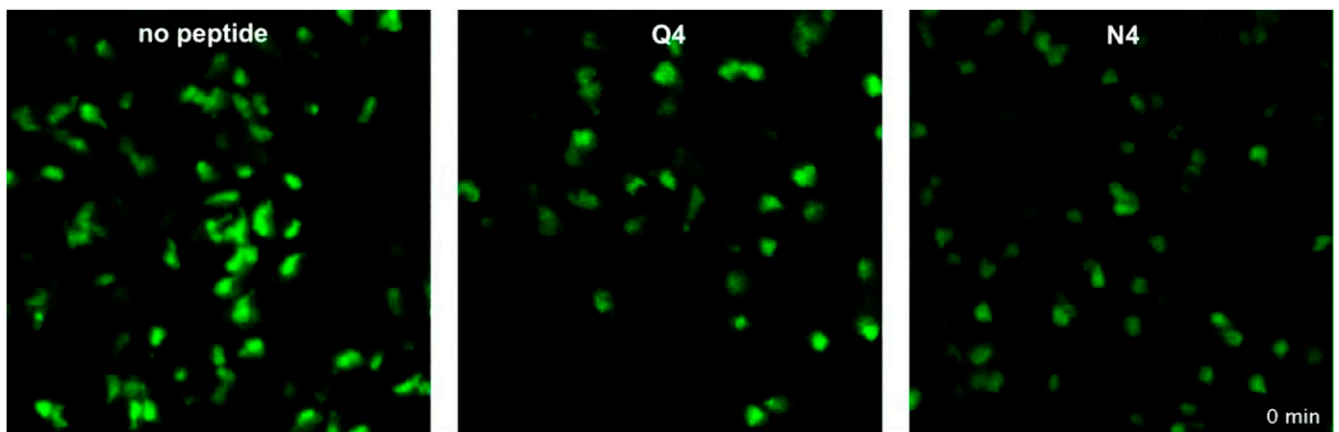
Fig. S7. Model of kinapse and synapse formation triggered by low- and high-affinity TCR ligands.
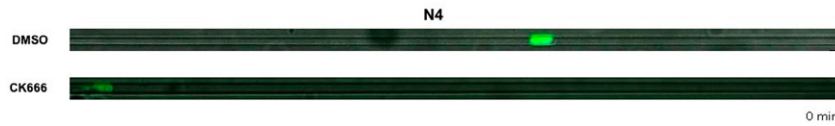

Movie S1. Distinct T-cell dynamics during recognition of high- and low-affinity TCR ligands in lymph nodes. Mice received transferred GFP$^+$ OT-I CD8$^+$ T cells, were injected with the high-affinity (N4) or the low-affinity (Q4) peptide, and were subjected to intravital imaging of the popliteal lymph node. Images were acquired every 30 s. Tracks over 5 min are shown in white.

[Movie S1](#)

Movie S2. Migration of GFP$^+$ OT-I CD8$^+$ T cells in pMHC-coated microchannels. Example of representative T cells migrating in microchannels coated with either K^b-TRP2, K^b-Q4, or K^b-N4 antigenic complexes. Images were acquired every 35 s.

[Movie S2](#)

Movie S3. Migration of GFP^{+} OT-I CD8^{+} T cells in K[b]-TRP2–coated microchannels in the absence or in the presence of EGTA. Images were acquired every 5 min.

[Movie S3](#)

Movie S4. Migration of GFP^{+} OT-I CD8^{+} T cells in K[b]-Q4–coated microchannels in the absence or in the presence of EGTA. Images were acquired every 5 min.

[Movie S4](#)

Movie S5. Migration of GFP^{+} OT-I CD8^{+} T cells in K[b]-N4–coated microchannels in the absence or in the presence of EGTA. Images were acquired every 5 min.

[Movie S5](#)

Movie S6. Migration of GFP^{+} OT-I CD8^{+} T cells in K[b]-TRP2–coated microchannels in the absence or in the presence of the Arp2/3 inhibitor CK666. Images were acquired every 3 min.

[Movie S6](#)

Movie S7. Migration of GFP^{+} OT-I CD8^{+} T cells in K[b]-Q4–coated microchannels in the absence or in the presence of the Arp2/3 inhibitor CK666. Images were acquired every 3 min.
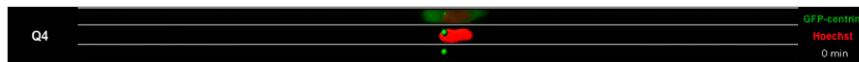
[Movie S7](#)

Movie S8. Migration of GFP+ OT-I CD8+ T cells in K^b-N4–coated microchannels in the absence or in the presence of the Arp2/3 inhibitor CK666. Images were acquired every 3 min.

[Movie S8](#)

Movie S9. Migration of GFP-centrin–expressing OT-I CD8+ T cells in K^b-TRP2–coated microchannels. First line: green, centrin-GFP; red, Hoechst. Second line: MTOC (green) and nucleus (red) tracking. Third line: MTOC trajectory. Images were acquired every 35 s.

[Movie S9](#)

Movie S10. Migration of GFP-centrin–expressing OT-I CD8+ T cells in K^b-Q4–coated microchannels. First line: green, centrin-GFP; red, Hoechst. Second line: MTOC (green) and nucleus (red) tracking. Third line: MTOC trajectory. Images were acquired every 35 s.
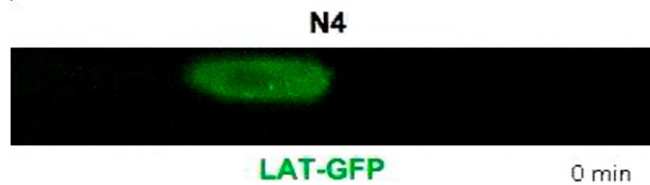
[Movie S10](#)

Movie S11. Migration of LAT-GFP–expressing OT-I CD8+ T cells in K^b-TRP2–coated microchannels, showing LAT at the uropod. Images were acquired every 3 min.

[Movie S11](#)

Movie S12. Migration of LAT-GFP–expressing OT-I CD8+ T cells in K^b-Q4–coated microchannels, showing changes in LAT polarity and punctuated LAT accumulations. Images were acquired every 3 min.
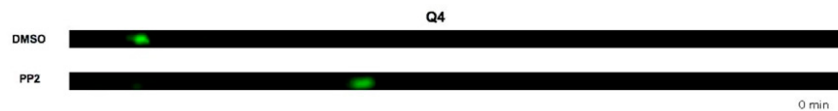
[Movie S12](#)

N4

LAT-GFP 0 min

Movie S13. Migration of LAT-GFP–expressing OT-I CD8$^+$ T cells in K^b-N4–coated microchannels, showing persistent punctuated LAT accumulations. Images were acquired every 3 min.
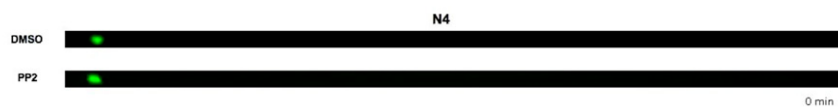
Movie S13

TRP2

DMSO

PP2

0 min

Movie S14. Migration of GFP$^+$ OT-I CD8$^+$ T cells in K^b-TRP2–coated microchannels in the absence or in the presence of the Src-family kinase inhibitor PP2. Images were acquired every 3 min.

Movie S14

Q4

DMSO

PP2

0 min

Movie S15. Migration of GFP$^+$ OT-I CD8$^+$ T cells in K^b-Q4–coated microchannels in the absence or in the presence of the Src-family kinase inhibitor PP2. Images were acquired every 3 min.

Movie S15

N4

DMSO

PP2

0 min

Movie S16. Migration of GFP$^+$ OT-I CD8$^+$ T cells in K^b-N4–coated microchannels in the absence or in the presence of the Src-family kinase inhibitor PP2. Images were acquired every 3 min.

Movie S16